Supporting Information

Stabilizing the Interface of $Li_{1.3}Al_{0.3}Ti_{1.7}(PO_4)_3$ and Lithium Electrodes via Interlayers Strategy in Solid-State Batteries

Jinhan Zhang,‡[a] Guixian Liu,‡*[a] Pengbo Zhai[ab] and Xiangxin Guo*[a]

[a.] College of Physics, Qingdao University, Qingdao 266071, China

[b.] Tianmushan Laboratory, Hangzhou 311115, China.

‡ The authors contributed equally to this paper.

*Corresponding authors

E-mail: liuguixian@qdu.edu.cn; xxguo@qdu.edu.cn

Abstract: The polyvinylidene carbonate:BN layer was constructed between $Li_{1.3}Al_{0.3}Ti_{1.7}(PO_4)_3$ (LATP) and the lithium (Li) electrode, improving interfacial compatibility and thermal stability. The Li_3N-rich solid electrolyte interphase regulates Li deposition behaviors. The solid-state Li metal batteries (SSLMBs) show remarkable electrochemical performance, exhibiting endurance for 800 hours of cycling at 0.2 mA cm^{-2} and critical current density of 1.4 mA cm^{-2}. These studies provide guidance for the interface engineering in SSLMBs.

Table of Contents

Experimental Procedures

1. Preparation of Solid-State Electrolytes. The NASICON-type $Li_{1.3}Al_{0.3}Ti_{1.7}(PO_4)_3$ (LATP) was synthesized via solid-state reaction. Specifically, the mixed powders with stoichiometric amounts of LiOH (99.99%, Aladdin), TiO_2 (99.9%, Aladdin), Al_2O_3 (99.9%, Macklin), and $NH_4H_2PO_4$ (99.9%, Aladdin) were ball-milled for 12 h. These precursor powders were dried for 12 h, and calcined in air at 450 ℃ for 2 h and 850 ℃ for 8 h. Then the LATP powders were obtained. Subsequently, the LATP powders were ball-milled for 12 h and then dried for 12 h to produce secondary powders. Finally, the secondary powders were pressed into pellets with the diameter of 12 mm by isostatic cool pressing, which were further polished by the sandpaper to get LATP pellets.

71.9 mg of lithium difluoro(oxalato)borate (LiDFOB, Macklin) and 13.6 mg of BN (98%, XFNANO) powders were added into 0.5 mL of vinylene carbonate (VC, Aladdin). The content of BN was 2 wt% corresponding to VC. The mixture was stirred at 500 rad min^{-1} for 12 h. Then 2.5 mg of azodiisobutyronitrile (AIBN, Aladdin) was added into the mixture as initiator which was further stirred at 500 rad min^{-1} for 30 min to obtain VC:BN dispersion. Such dispersion was coated onto the LATP pellets with the spin coater to obtain the VC:BN-LATP pallets. The polymerization of VC:BN was completed in the following assembling process of Li metal batteries.

2. Fabrication of Li-Li Symmetric Cells and Solid-State Batteries. All the assembling of the Swagelok-type cells were carried out in the argon-filled glovebox (H_2O < 0.1 ppm, O_2 < 0.1 ppm). The VC:BN-LATP pellets were sandwiched between two Li metal sheets to fabricate the Li-Li symmetric cells. They were constantly kept at 60 °C for 6 h in the drying oven to make VC completely polymerized. The obtained Li|PVC@BN-LATP|Li symmetric cells were. The cells underwent the resting time of 12 h before testing. In addition, Li|LATP|Li symmetric cells were also assembled for comparison.

In order to prepare the $LiFePO_4$ cathodes, the $LiFePO_4$ powder (LFP, 80 wt%), Super P carbon (10 wt%) and polyvinylidene fluoride (PVDF, 10 wt%) were dispersed in moderate N-methyl-2-pyrrolidone (NMP) to obtain slurries. The slurries were milled

for 30 min and then coated on the aluminum (Al) foils. They were dried for 12 h in the vacuum oven at 80 °C to remove the solvent. The load of active materials is about 1.8~2.0 mg cm^{-2}. Using Li metal as the anode and LFP as the cathode, the Li|PVC@BN-LATP|LFP and Li|LATP|LFP full cells were assembled respectively.

3. Material Characterizations. The X-ray diffraction (XRD, Rigaku Smart II) was employed to detect the phase structure of LATP and PVC:BN-LATP with the range of 2θ set as 10°~80°. The morphologies of LATP, BN and PVC:BN-LATP were observed by field emission scanning electron microscopy (SEM, FEI Verios G4). The SEM was also applied to disclose the surface morphology of the LATP and Li electrode, as well as the cross-section morphology of the Li/LATP interface before cycling and after cycling at the 0.1 mA cm^{-2} (0.1 mAh cm^{-2}) at 30°C for 100 h. When characterizing the morphology of the LATP surface in the PVC:BN-LATP-based cell, the interlayer was carefully detached from the LATP surface. To obtain the LATP pellet with a clean surface, the separated LATP pellet was subsequently subjected to ultrasonic cleaning in alcohol to eliminate any residual PVC:BN coating. The X-ray photoelectron spectroscopy (XPS) experiments were performed using a PHI 5000 Versa Probe scanning ESCA microprobe (Physical Electronics) to study the composition of the interlayer and the interfacial chemistry between the Li anode and distinct solid-state electrolytes before cycling and after cycling at the 0.1 mA cm^{-2} (0.1 mAh cm^{-2}) at 30 °C for 100 hours. Fourier-transform infrared (FT-IR) spectroscopy (Thermo Fisher Scientific Nicolet iS10) was applied to analyze the formation of VC, PVC and PVC:BN. The distribution of particle size was analyzed using the laser particle size analyzer (Brookhaven Zeta Plus). Thermal stability tests of LATP and PVC:BN-LATP were conducted using Li|LATP and Li|PVC:BN-LATP systems in the Ar-filled glovebox. The Li metal was placed on the stainless-steel heating plate. The LATP or PVC:BN-LATP pellet was placed onto the Li metal. The thermal infrared camera (FOTRIC 266-2) was adopted to acquire the thermal infrared image of the Li|LATP and Li|PVC:BN-LATP pellets.

4. Electrochemical Tests. The charge-discharge cycling tests of solid-state Li metal

batteries were performed at various current densities or rates using the NETWARE battery analyzer (CT-4008Tn). The galvanostatic charge-discharge tests for the symmetric batteries were carried out at 0.1 and 0.2 mA cm^{-2}, and each cycle was lasted for 1 h. The CCD tests were carried out under step-increased current densities with a step of 0.05 mA cm^{-2} and a fixed charge/discharge time of 0.5 h. The ionic conductivity of LATP and PVC:BN-LATP and the interfacial impedance in Li|LATP|Li and Li|PVC:BN-LATP|Li cells were explored by potentiostatic electrochemical impedance spectroscopy (EIS) on the PARSTAT 3000A electrochemical workstation (Princeton). The full cells coupled with LFP are cycled at 0.1 C and 0.2 C at the potential of 2.5~3.7 V to evaluate the cycling performance. The rate performance was evaluated from 0.05 C to 0.5 C. All electrochemical tests were performed at 30 °C.

Supporting Figures

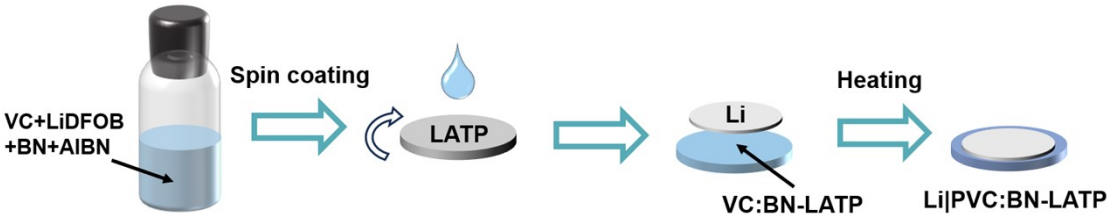

Fig. S1 The schematic of preparing the PVC:BN-coated LATP.

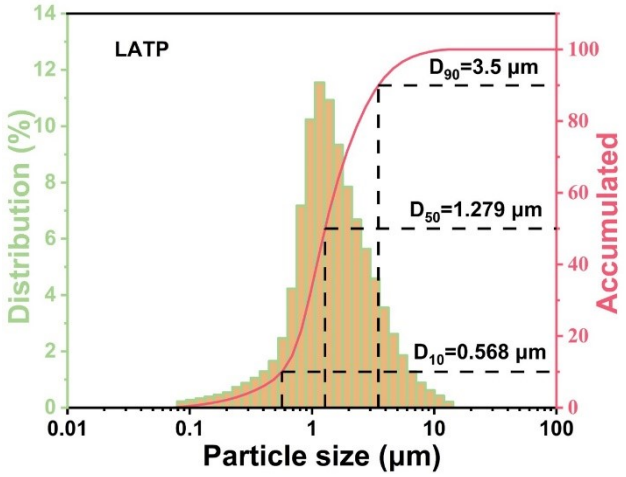

Fig. S2 The size distribution of LATP particles. The D10, D50 and D90 are calculated as 0.568 μm, 1.279 μm and 3.5 μm.

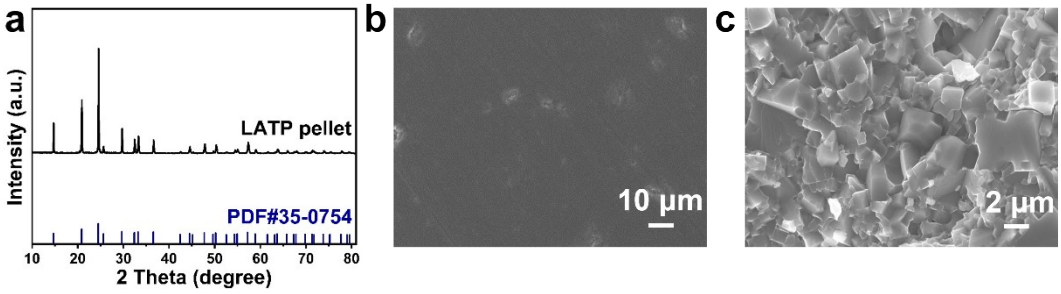

Fig. S3 (a) The XRD patterns of the LATP pallet. The SEM images of the (b) surface and (c) cross-section of the LATP pellet.

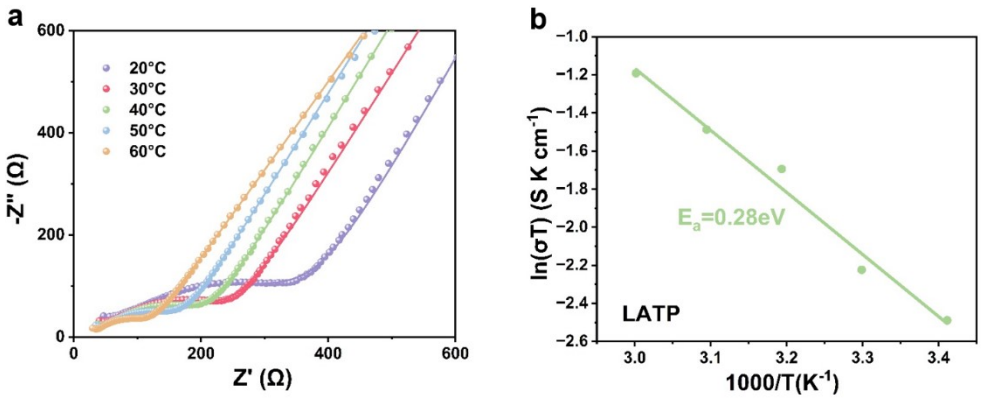

Fig. S4 (a) The EIS spectra of the Au|LATP|Au cells at various temperatures. (b) The Arrhenius plot of the LATP pellets. The activation energy is calculated as 0.28 eV.

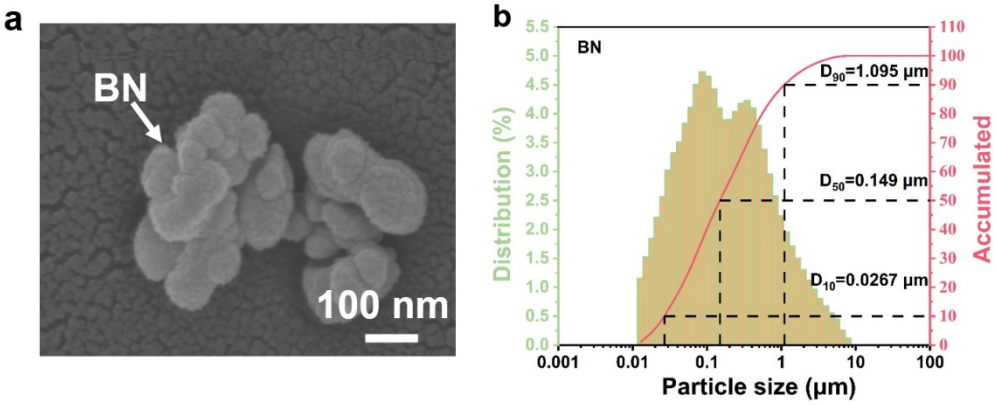

Fig. S5 The (a) SEM image and (b) size distribution of BN particles. The D10, D50 and D90 are 0.568 μm, 1.279 μm and 3.5 μm respectively.

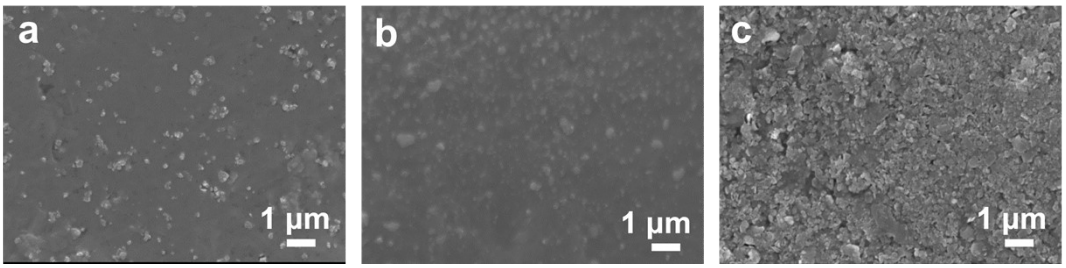

Fig. S6 The SEM images of the surface of PVC-based composite layer with (a) 0.5 wt %, (b) 1 wt % and (c) 3 wt % of BN.

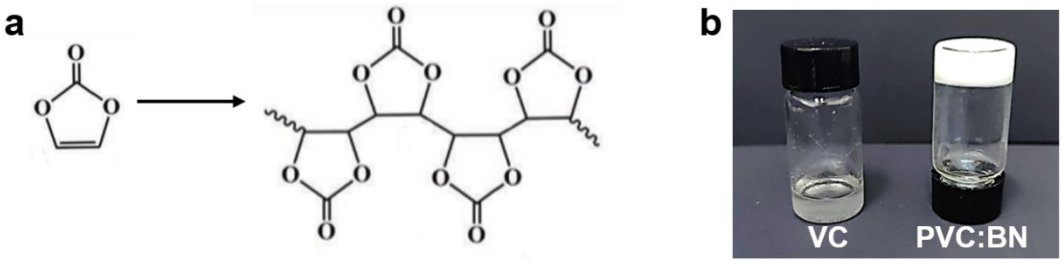

Fig. S7 (a) The reaction mechanism of VC. (b) The digital images of in-situ polymerization of VC into PVC:BN after heating at 60 °C for 24 h.

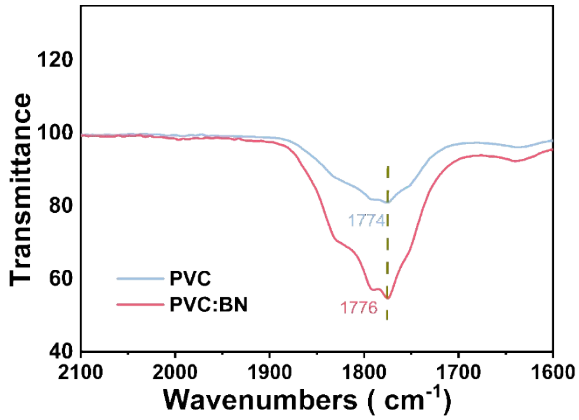

Fig. S8 The FT-IR curves of PVC and PVC:BN.

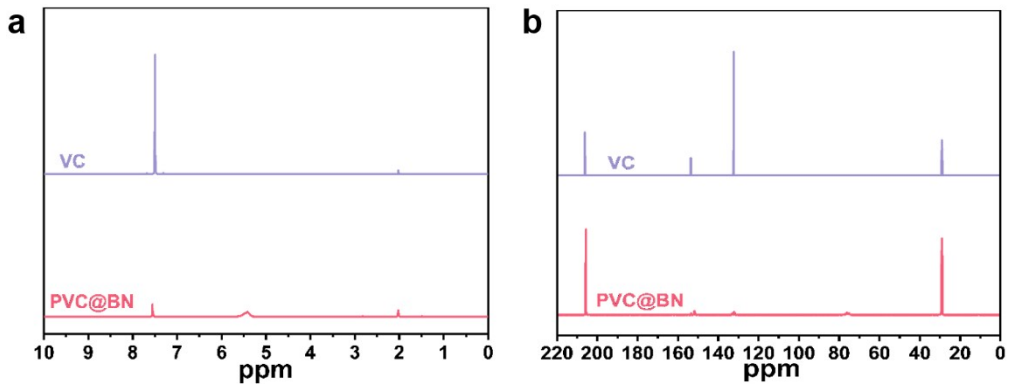

Fig. S9 (a) ^{1}H and (b) ^{13}C NMR spectra of VC and PVC:BN in Acetone-d6.

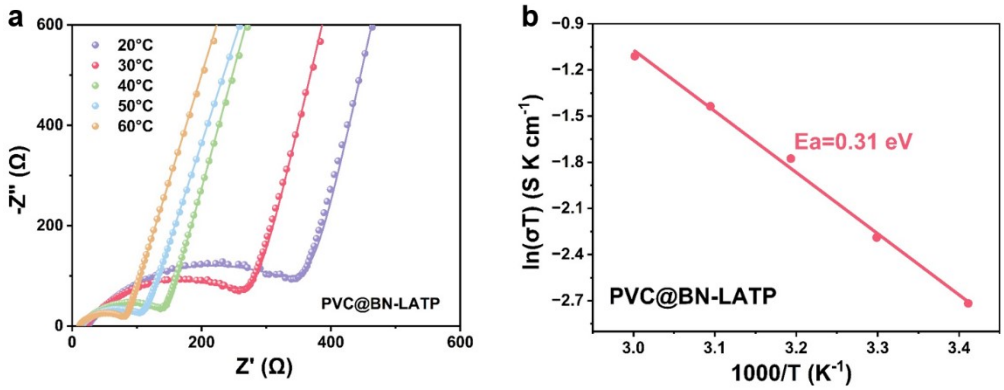

Fig. S10 (a) Nyquist plots of the Au|PVC:BN-LATP|Au symmetrical cells. (b) The corresponding Arrhenius plot of the ionic conductivities.

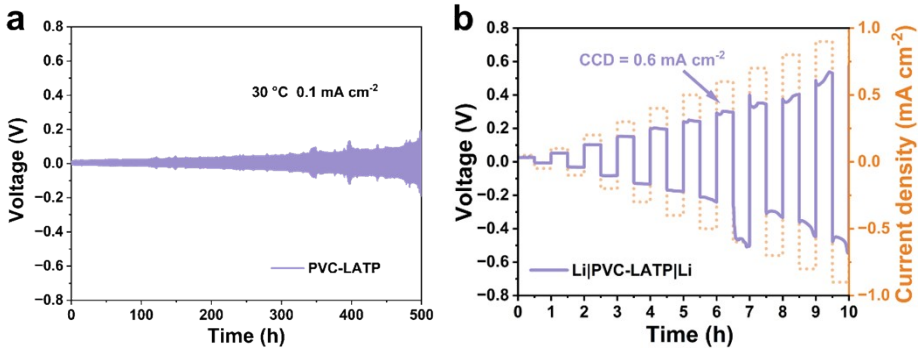

Fig. S11 (a) The galvanostatic curves of Li|PVC-LATP|Li cells under 0.1 mA cm^{-2}. (b) The CCD curves of Li|PVC-LATP|Li cells.

As shown in Fig. S11, the performance of Li|PVC-LATP|Li cells is improved. The performance improvement of cells with the PVC interlayer can be attributed to two primary factors: (1) The PVC interlayer effectively isolates LATP from direct contact with the Li metal electrode and guarantees the well-connected and continuous pathway for ion transport. (2) From the XPS spectra in Figure 3k in the Main Text, a significant presence of LiF has been observed on the surface of the Li electrode in the PVC-LATP-based cell, which is ascribed to the decomposition of the LiDFOB in the electrolyte. The LiF-rich SEI film further regulates the Li deposition uniformity, promoting the interfacial performance of cells with PVC interlayer.[1]

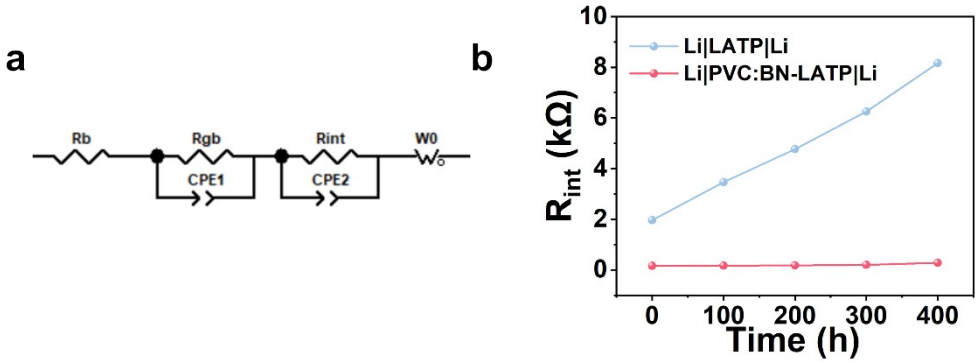

Fig. S12 (a) The corresponding equivalent circuit and (b) interfacial resistance data of Li|LATP|Li and Li|PVC:BN-LATP|Li cells after different cycling times at 0.1 mA cm^{-2}.

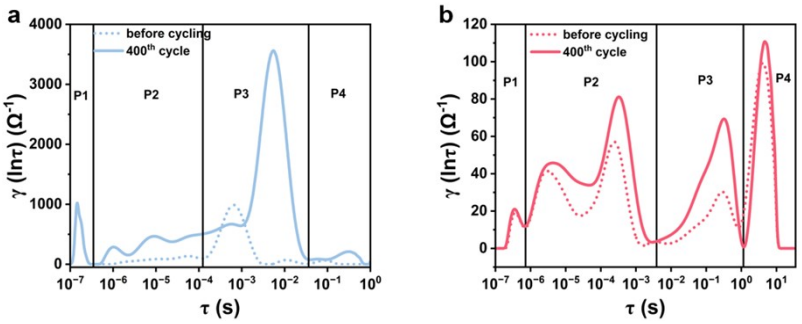

Fig. S13 The DRT plots for the (a) Li|LATP|Li system and (b) Li|PVC:BN-LATP|Li system before and after cycling.

Fig. R5 illustrates the DRT plots of the Li|LATP|Li and Li|PVC:BN-LATP|Li systems before and after cycling. For the Li-Li symmetrical cells with solid-state electrolytes, the four polarization regimes can be distinguished by their respective relaxation times: electrical double layer capacitance (P1), grain boundary (P2), interfacial charge transfer (P3) and solid-state diffusion (P4).[2,3] Apparently, for the Li|LATP|Li and Li|PVC:BN-LATP|Li systems, both the grain boundary resistance and interfacial charge transfer resistance of the cells after cycling are increased than the cells before cycling, indicating the gradual interfacial degradation. And the grain boundary resistance and interfacial charge transfer resistance of the Li|PVC:BN-LATP|Li cells are decreased as compared with the Li|LATP|Li cells, distinctly disclosing the interfacial improvement after introducing the PVC:BN interlayer.

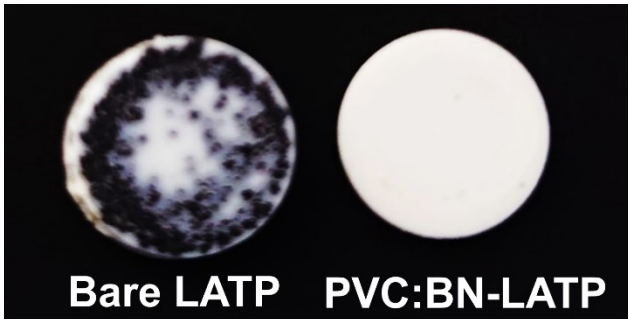

Fig. S14 Optical images of the surface of bare LATP and PVC:BN-LATP after 100 cycles.

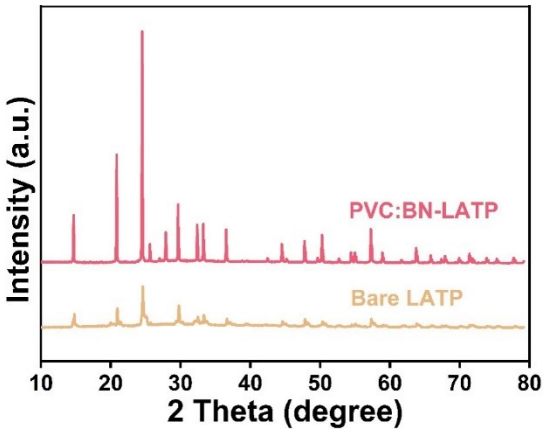

Fig. S15 XRD patterns of the surface of bare LATP and PVC:BN-LATP after 100 cycles.

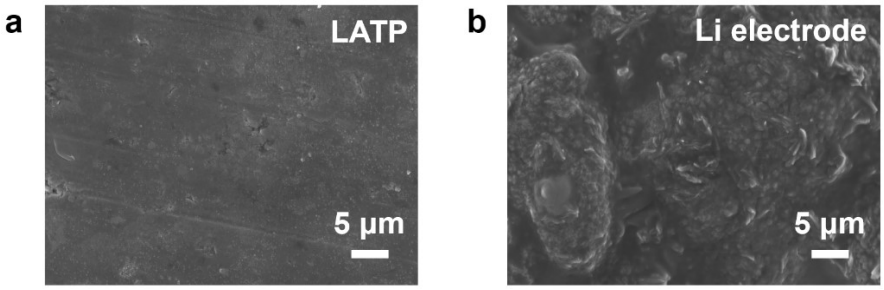

Fig. S16 SEM images of the (a) LATP and (b) Li surface in PVC-LATP-based cells after cycling.

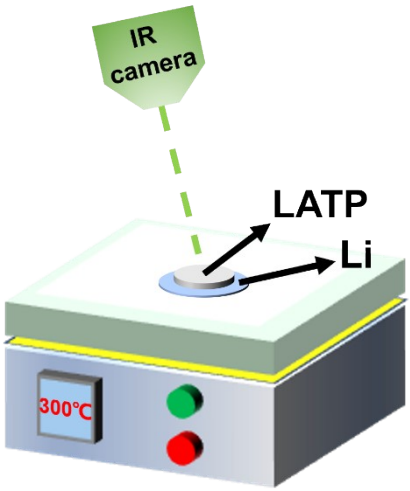

Fig. S17 The schematic illustration of the thermal runaway measurements of the metallic Li and LATP at high temperatures.

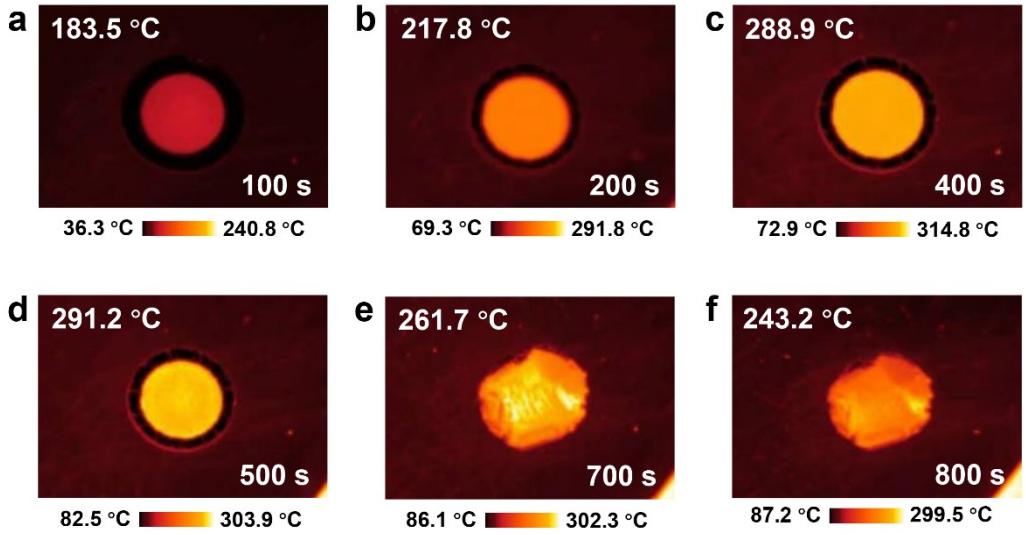

Fig. S18 The thermal infrared images of the Li|LATP system after heating for different times.

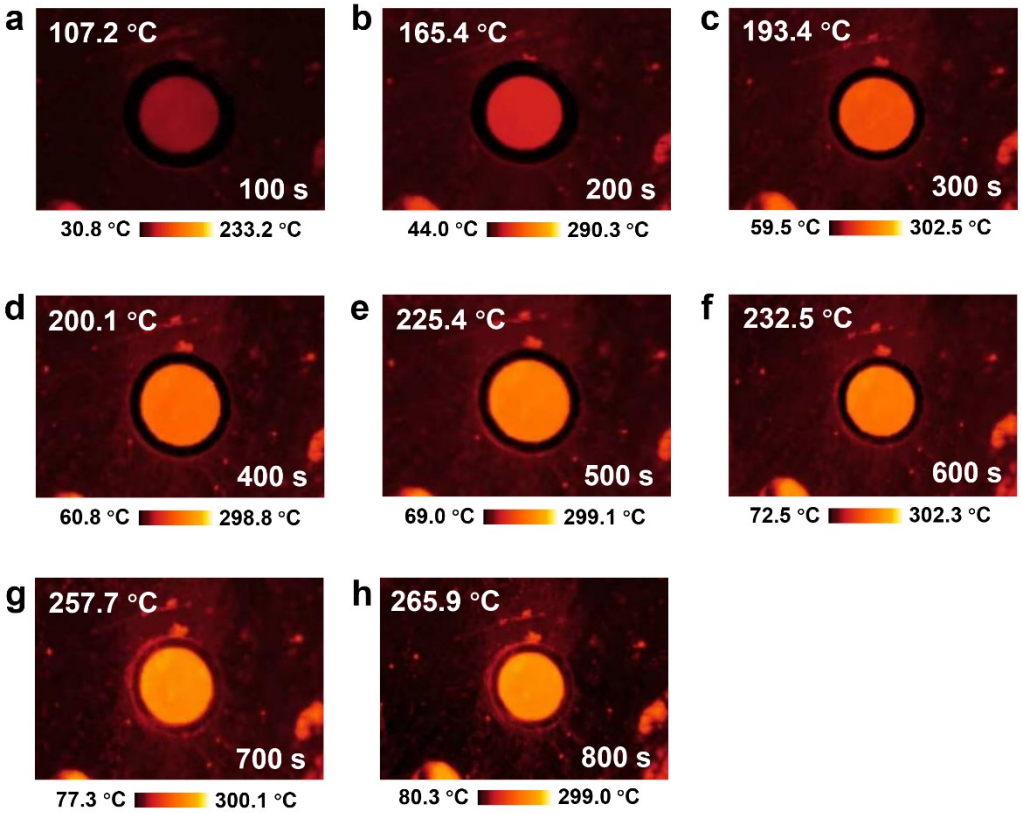

Fig. S19 The thermal infrared images of the Li|PVC-LATP system after heating for different times.

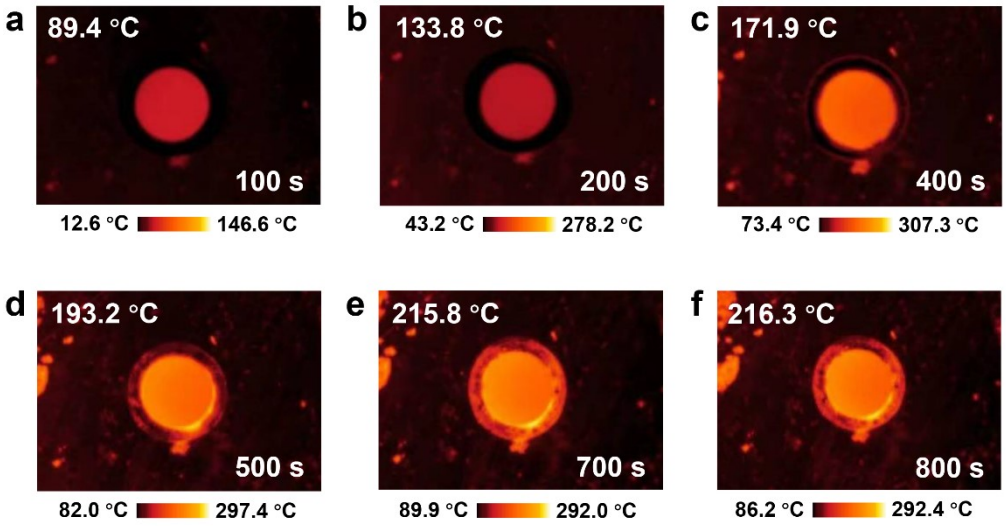

Fig. S20 The thermal infrared images of the Li|PVC:BN-LATP system after heating for different times.

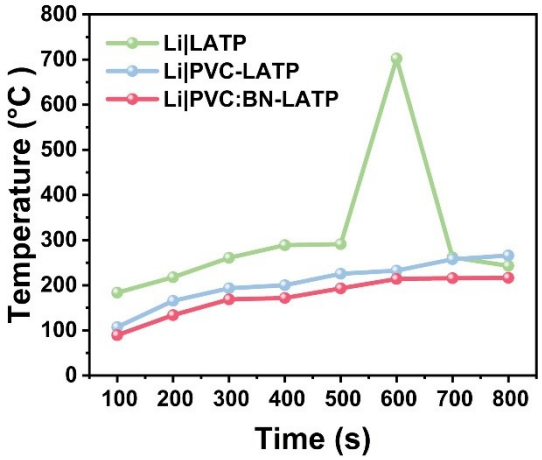

Fig. S21 The temperature changing profiles of Li|LATP, Li|PVC:BN-LATP and Li|PVC-LATP systems.

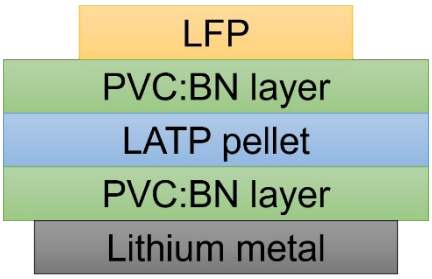

Fig. S22 The schematic illustration of the fabrication of Li|PVC:BN-LATP|LFP cells.

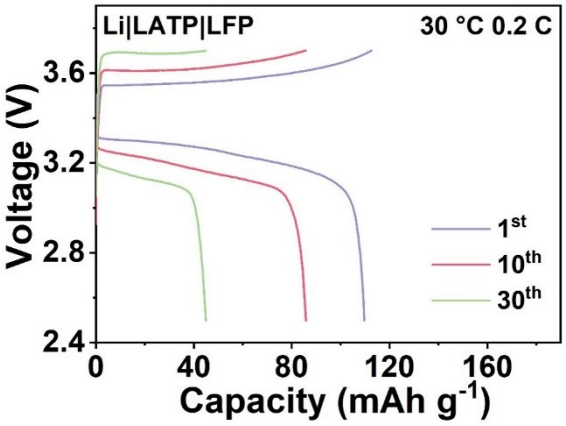

Fig. S23 The charge/discharge curves of Li|LATP|LFP batteries at 0.2 C.

Supplementary Tables

Table S1. Related data of the relative density of the prepared LATP pallets.

Sample No.	m_0 /g	ρ_e /(g·cm^{-3})	m_1 /g	ρ /(g·cm^{-3})	ρ_0 /(g·cm^{-3})	ρ_r /%
1	0.1993	0.7876	0.1430	2.7881	2.947	94.60
2	0.1907	0.7876	0.1371	2.8038	2.947	95.14
3	0.1894	0.7876	0.1359	2.7923	2.947	94.75
4	0.1955	0.7876	0.1398	2.7655	2.947	93.84

The density (ρ) of prepared LATP pallets was measured by the Archimedes' drainage method according to the following equation:

$$\rho = \rho_e \frac{m_0}{m_0 - m_1}$$

In this equation, m_0 refers to the mass of the solid electrolyte in the air, m_1 refers to the mass of the solid electrolyte immersed in absolute ethanol, and ρ_e is the theoretical density of absolute ethanol (0.7876 g cm^{-3}, 22°C). Subsequently, the relative density (ρ_r) of the LATP pallets was further calculated according to the following equations:

$$\rho_r = \frac{\rho}{\rho_0} \times 100\%$$

In the equation, ρ_0 is the theoretical density of solid electrolyte, which can be calculated by the following formula:

$$\rho_0 = \frac{M}{N_A \times V}$$

Among them, M is the molar mass of the solid electrolyte, N_A is Avogadro's constant, and V represents the theoretical unit cell volume of the solid electrolyte.

According to this method, the average ρ and ρ_r of the LATP pallets are calculated as 2.79 g·cm^{-3} and 94.58% respectively, suggesting that the prepared LATP pallets feature a high density.

References

1. P. X. Bai, X. Ji, J. X. Zhang, W. R. Zhang, S. Hou, H. Su, M. J. Li, T. Deng, L. S. Cao, S. F. Liu, X. Z. He, Y. H. Xu and C. S. Wang, *Angew. Chem. Int. Ed.*, 2022, 61, e202202731.
2. Y. Lu, C. Z. Zhao, J. Q. Huang and Q. Zhang, *Joule*, 2022, **6** (6), 1172-1198.
3. D. Park, S. Shin, P. C. Sherrell, B. Roy, K. L. Callaghan, F. Caruso and A. V. Ellis, *Adv. Funct. Mater.*, 2024, 2417549.